A. EFIMOV ✉
A.J. TAYLOR

Spectral-temporal dynamics of ultrashort Raman solitons and their role in third-harmonic generation in photonic crystal fibers

Materials Science and Technology Division, MST-10, MS K764, Los Alamos National Laboratory, Los Alamos, NM 87545

ABSTRACT We use cross-correlation frequency-resolved optical gating to obtain spectral-temporal portraits of ultrashort Raman solitons in photonic crystal fibers at telecommunication wavelengths. Power-dependent Raman frequency shifts of 200 nm in 63 mm of fiber are observed accompanied by spectral broadening and 2.5-times soliton compression. Complete time-frequency dynamics at the fundamental wavelength thus visualized enables us to explain the details of the intermodally phase-matched third harmonic generation by the propagating solitons.

PACS 42.65.Ky; 42.65.Re; 42.65.Sf; 42.65.Tg; 42.65. Wi; 42.81. Dp

1 Introduction

The nonlinear dynamics of ultrashort optical pulses in photonic crystal fibers (PCF) [1] continues to bring surprises and display rich phenomena such as supercontinuum [2] and intermodally phase-matched third harmonic generation (THG) [3], unusual solitonic regimes [4], Cherenkov continuum generation and soliton stabilization [5], generation of very high-order UV modes [6], scattering of continuous waves on solitons [7] and others. Soliton dynamics in PCFs is currently believed to play a fundamental role in supercontinuum generation through soliton fission, Raman self-frequency shifts and emission of phase-matched non-solitonic (Cherenkov-type [8]) radiation across the zero-dispersion point [9]. Solitonic behavior was observed in PCFs throughout the range of anomalous dispersion in the infrared and Raman solitons were proposed for sources of tunable femtosecond radiation [10–13]. All of the previous observations of Raman solitons in PCFs (as well as other optical fibers) were performed with time-integrated spectral measurements and in some cases with autocorrelation techniques. In a recent work by Konorov et al. [14], cross-correlation type measurements were performed, however no clear solitonic features were observed. In this work we present time-spectrally re-

solved dynamics of Raman solitons in cob-web PCFs with unprecedented resolution, dynamic range and exceptionally low noise. These results serve not only as a clear visualization of solitonic propagation at the fundamental wavelength, but also elucidate the exact processes responsible for intermodally phase-matched third harmonic generation [3].

For detailed studies of optical pulse propagation in optical fibers in the nonlinear regime simple spectral measurements become insufficient. Even autocorrelation-based measurements such as frequency-resolved optical gating (FROG) [15] are inadequate because the two-dimensional traces resulting from such measurements are symmetric in time and thus not very intuitive and posses intrinsic ambiguities. From the point of view of obtaining experimentally the most complete picture of the pulse dynamics, reference-type measurement is needed. An approach which we believe is ideally suitable for studying the ultrafast pulse dynamics in optical fibers, including PCFs, is the cross-correlation frequency-resolved optical gating (X-FROG) [16]. X-FROG has already been used for studies of soliton propagation in regular fibers and PCFs [17, 18]; however, the relative complexity of the setup so far precluded the wide proliferation of the technique. Here we present time-spectrally-resolved measurements of Raman soliton dynamics in a short piece of PCF at telecom wavelengths showing unambiguously the expected solitonic features for the first time. The observed time-resolved dynamics further deepens our understanding of the process of intermodally phase-matched THG in PCFs [3] previously argued with spectral measurements only.

2 Experimental setup

The PCFs used in our experiments, Fig. 1, are made from pure silica and in their optical properties are very similar to the single strand of silica suspended in air. The most crucial parameter of the PCF is the central guiding core diameter, which was 2.5 µm in our case. Among other things the central core size determines the zero dispersion wavelength, typically located in the red or near-infrared portion of the spectrum. Exact location of the zero dispersion point on the wavelength axis is not important in our case, since we pump the fiber well in the anomalous dispersion region at the telecom wavelengths. The length of the PCF was 63 mm, although other lengths as well as core sizes were used in our previous experiments [3, 6].

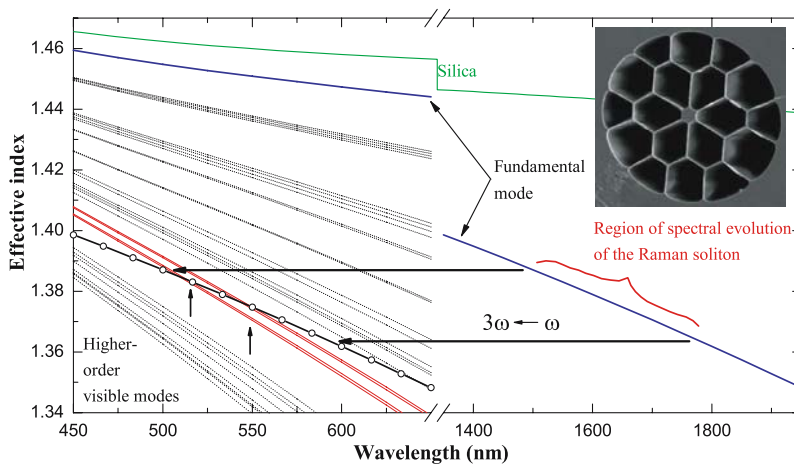✉ Fax: +1-425-963-2699, E-mail: efimov@lanl.gov

FIGURE 1   Modal portrait of the PCF used in the experiments and the mechanism of intermodally phase-matched THG. (*Topmost green curve*) is the refractive index of silica; blue curve—fundamental mode of the fiber; (*thin grey curves*)are higher-order modes in the visible; (*red curves*)—visible modes to which the fundamental mode phase matches for THG process; (*black curve with open circles*)—fundamental mode shifted by 3ω to the visible to show phase-matching conditions (*vertical arrows*). (*Inset*)—SEM image of the fiber cross section

We performed full-vectorial numerical modeling of the dispersion and modal properties of our PCF using the scanning electron microscope image of the input cleave of the fiber. The simulations, Fig. 1, indicate that the fiber is multimode even at the pump wavelength of 1550 nm (only the fundamental mode in the infrared is shown) and becomes more so at shorter wavelengths. At these conditions various intermodally phase-matched nonlinear processes become possible [19] one of which is the THG when the fundamental mode at the fundamental wavelength is phase-matched to a higher-order mode in the visible, see Fig. 1. The dynamics of the fundamental pulse plays an important role in this process since the input pulse undergoes soliton formation and strong self-frequency shift during propagation. Phase-matching conditions are, thus, dynamic and changing along the fiber. Frequency shifting solitons if not initially phase-matched to a specific higher-order mode at the 3ω frequency may become phase-matched later during propagation.

The experimental setup, Fig. 2, for studying the time-frequency-resolved Raman soliton dynamics includes an optical parametric oscillator (OPO) synchronously pumped by a femtosecond Ti:sapphire laser (Spectra Physics Millenia, Tsunami and Opal). The output pulses of 100 fs duration follow in a pulse train at 82 MHz repetition rate and average powers up to 350 mW. The OPO tuning range is 1400–1600 nm. Pulses from the OPO are split in the reference and signal arms where the former propagates in a self-retracing variable delay apparatus and the latter is input into a fiber under study through the polarization and power control optics using an aspheric lens. Typical coupling efficiency was about 50 percent. The output from the fiber is mixed with a transform-limited reference pulse in a 200 μm thick BBO crystal and the sum-frequency signal is spectrally-resolved in a 0.3 nm resolution spectrometer. The

phase-matching bandwidth of the BBO crystal at the central wavelength of 1550 nm exceeds 400 nm and is sufficient to upconvert the whole spectrum of the signal pulse.

The result of an X-FROG measurement is a two-dimensional image, a spectrogram, that shows the portrait of the pulse simultaneously in time and frequency [16]. Thus, the spectrogram can be interpreted as displaying relative temporal positions of various frequency components comprising the signal pulse. This portrait is an indispensable tool for imaging the structure of complex optical pulses. Currently there is even a trend for using spectrograms in theoretical and numerical work [4], rather than showing separate spectral and temporal profiles for the pulse. In simple terms an X-FROG trace is a spectrally-resolved cross-correlation of the signal and reference pulse:

$$I_{\text{X FROG}}(\omega, \tau) = \left| \int_{-\infty}^{+\infty} E(t) E_{\text{ref}}(t - \tau) \exp^{-i\omega t} \, dt \right|^2 \qquad (1)$$

where $I_{\text{X FROG}}(\omega, \tau)$ is the intensity of the X-FROG signal as a function of optical frequency ω and delay τ between signal $E(t)$ and reference $E_{\text{ref}}(t - \tau)$ pulses. Expression (1) written for so-called sum-frequency generation X-FROG is easy to understand: the product of two fields is obtained through the process of sum-frequency generation in a thin crystal with quadratic nonlinearity and the Fourier transform is obtained using a spectrometer. The focal plane detector of the spectrometer measures the spectral intensity; hence, the spectrogram is proportional to the modulus squared of the spectrum of the sum-frequency generated signal. Special algorithms can be used to recover the complete temporal behavior of the electric field, or equivalently, the amplitude and the phase of the optical pulse in either temporal or spectral domains. The information conveyed by the spectrogram allows one to grasp the whole picture of a complex ultrashort pulse.
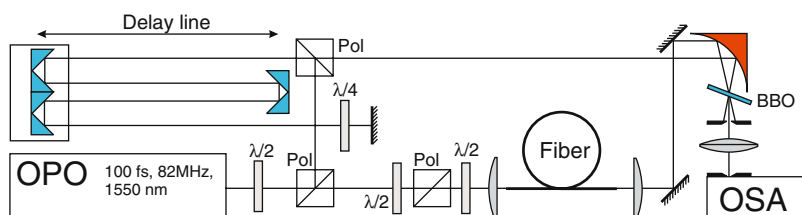

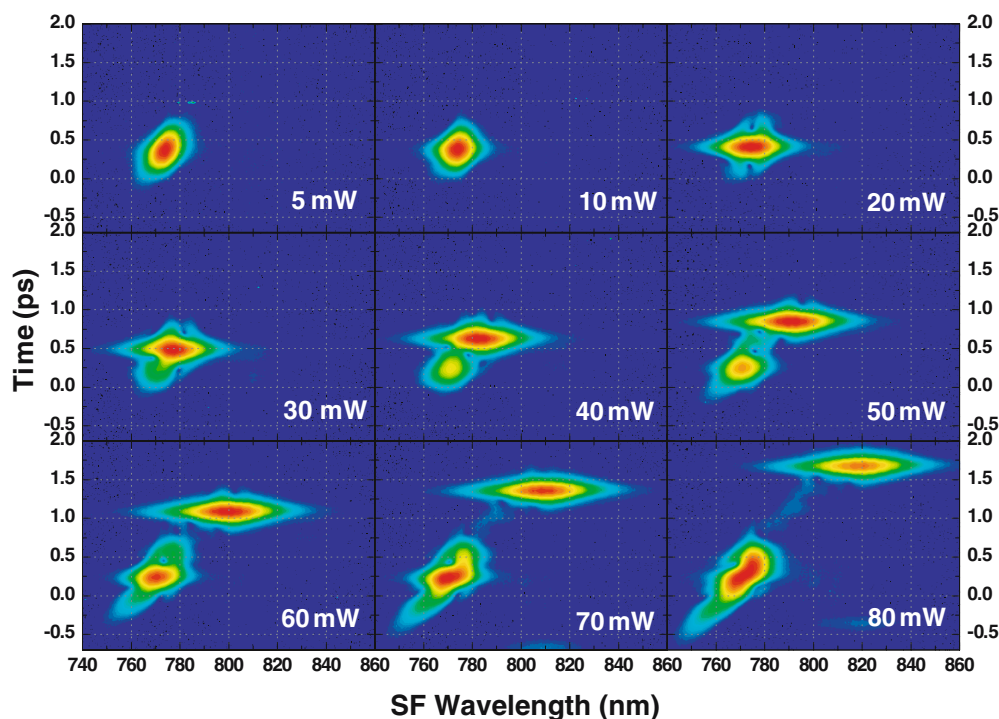FIGURE 2   Schematic of the X-FROG setup used in the experiments

FIGURE 3 Experimental power-dependent X-FROG traces at the output of 2.5 μm core PCF, 63 mm in length. Soliton formation, pulse splitting and Raman self-frequency shift are clearly seen. Color scale is *logarithmic* in intensity of sum-frequency signal. The horizontal axis corresponds to sum-frequency signal wavelength. For each trace input average powers are shown

3   Results and discussion

Figure 3 shows a series of X-FROG traces recorded at the output of the PCF for varying input powers of the pump pulse. The input wavelength is located well within the anomalous dispersion region of this fiber so no supercontinuum generation is observed. At high powers, however, intermodally phase-matched THG occurs, Fig. 4 [3]. At 5 mW the propagation of the fundamental pulse is nearly linear which can be inferred from the elliptical shape of the trace as well as parabolic phase from X-FROG reconstruction, Figs. 5 and 6, in both temporal and spectral domains. Soliton formation sets in at about 10 mW, at which point the X-FROG trace assumes the required diamond-like shape, characteristic to the Sech(t) temporal amplitude profile. We note here that the reference pulse coming out of the OPO also has the Sech(t) shape as was verified in a separate FROG measurement. Spectral and temporal phase functions, Figs. 5 and 6 show substantial flattening, as expected, for 10 mW and 20 mW input power cases. With further increasing of the input power, pulse splitting and Raman self-frequency shift of the main soliton can be clearly seen. The frequency shifting soliton maintains the diamond-like X-FROG shape which is a clear evidence for the solitonic Sech(t) amplitude profile. From the reconstructed phase functions, we see that the Raman soliton remains flat-phased (the tilt of the phase function corresponds to linear shift on the time axis), whereas the pulse remaining in the vicinity of the pump wavelength is, in fact, chirped, as evidenced by the curved phase in Fig. 6. The wavelength shift of the Raman soliton is accompanied by the delay offset in accordance with the anomalous dispersion of the fiber: red-shifting soliton is delayed with respect to the non-shifted pulse near
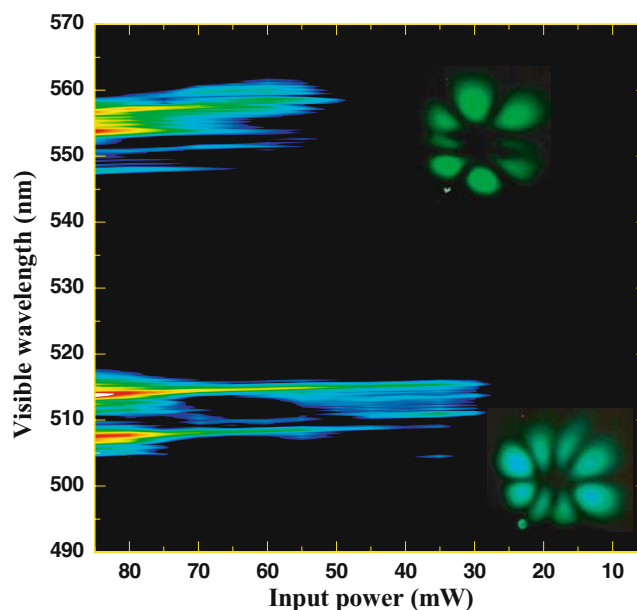

FIGURE 4 Power-dependent THG spectra at the output of the PCF. Two doublets are observed around 510 nm and 550 nm. The spectral position of the visible harmonics are in agreement with analysis of Fig. 1. Experimental far-field intensity profiles of the modes are shown next to the respective spectra. Two modes within each pair are nearly-degenerate and have almost identical far-field distributions. Color scale is logarithmic

the fundamental wavelength. Note that in 63 mm of fiber the Raman soliton experiences 200 nm of wavelength shift at the highest input power. With increasing input power the spectral width of the Raman soliton increases and at the same time the temporal duration of the soliton decreases since the Raman
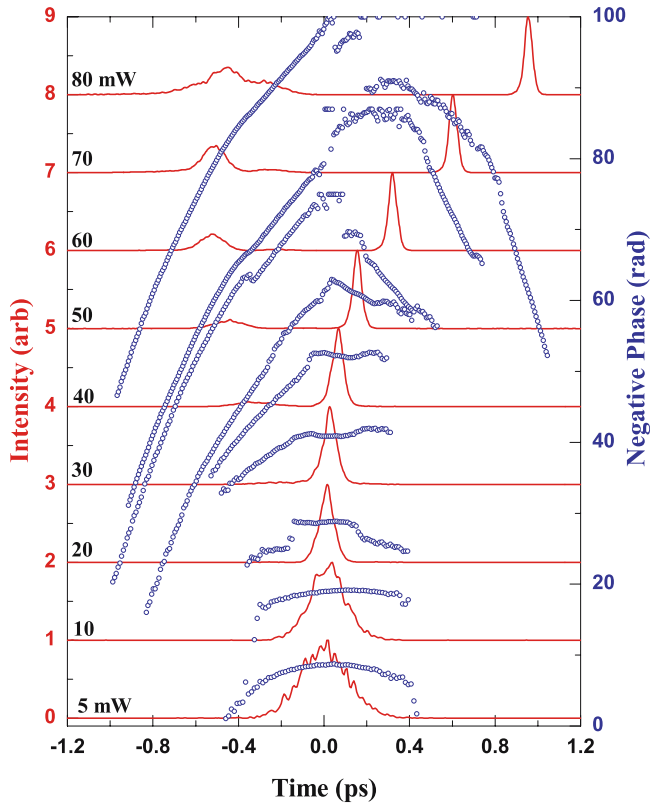
FIGURE 5 Intensity (*red curves*) and phase (*blue circles*) of the pulse in time domain at the output of the PCF reconstructed from the experimental X-FROG spectrograms. Reconstruction error does not exceed 0.002 on 256 × 256 grid for all power levels
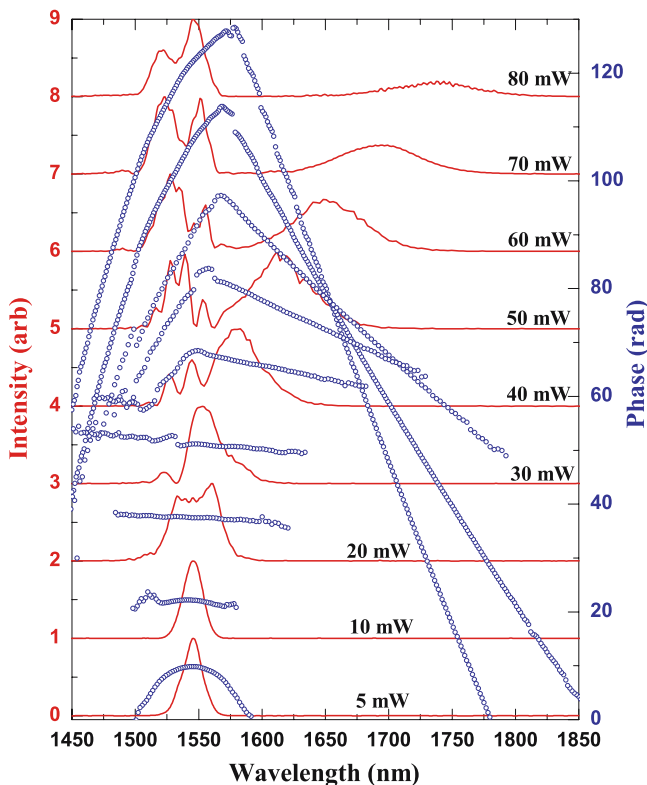

FIGURE 6 Intensity (*red curves*) and phase (*blue circles*) of the output pulse in spectral domain. Input power increases from bottom to top, as in Fig. 5

soliton constitutes a transform-limited pulse. At the 80 mW input power the intensity full-width at half-maximum of the Raman soliton reaches 42 fs, which gives the soliton compression ratio of 2.5 times with respect to the input pulse duration. Finally, we note the formation of temporal π-phase slips at 30 mW previously observed with FROG for solitons forming in regular fibers [20].

Analysis of the THG spectra, Fig. 4 indicates that a pair of nearly-degenerate modes around 510 nm is generated at low input power. These modes are emitted directly by the input pulse through one of the phase-matching conditions shown in Fig. 1. The second pair of modes around 550 nm can not be emitted by the input pulse because spectral component at 1650 nm is required and not originally present in the input pulse spectrum. Indeed, these modes become visible only at 50-60 mW of input power. Generation of these modes becomes possible through the other phase-matching condition of Fig. 1 by the Raman soliton, which reaches 1650 nm at 50–60 mW at the end of the fiber, see Fig. 6. At higher powers generation of 550 nm modes is also possible since the Raman soliton reaches phase-matching wavelength earlier within the fiber. Finally, we note that the complex structure of the visible modes' spectral lines can be attributed to the cross-phase modulation during THG [21, 22].

4   Conclusion

We visualized the Raman soliton dynamics in the anomalous dispersion region of a PCF at telecommunication wavelengths with cross-correlation frequency-resolved optical gating. Time-spectrally resolved images of Raman solitons were obtained for varying input powers of the pump pulse and detailed dynamics of pulse splitting, self-frequency shifts and soliton compression were clearly observed. Frequency-shifting Raman soliton is responsible for the generation of the 550 nm doublet of nearly degenerate visible modes, whereas the modes at 510 nm are generated directly by the input pulse near the beginning of the fiber. We believe that further application of X-FROG to ultrashort pulse dynamics in PCFs will deepen our understanding of many phenomena observed previously with spectral measurements and lead to new discoveries in this field [7].

REFERENCES

1 W.H. Reeves, D.V. Skryabin, F. Biancalana, J.C. Knight, P.St.J. Russell, F.G. Omenetto, A. Efimov, A.J. Taylor, Nature **424**, 511 (2003)
2 J.K. Ranka, R.S. Windeler, A.J. Stentz, Opt. Lett. **25**, 25 (2000)
3 A. Efimov, A.J. Taylor, F.G. Omenetto, J.C. Knight, W.J. Wadsworth, P.St.J. Russell, Opt. Express **11**, 2567 (2003)
4 G. Genty, M. Lehtonen, H. Ludvigsen, Opt. Express **12**, 4614 (2004)
5 D.V. Skryabin, F. Luan, J.C. Knight, P.St.J. Russell, Science **301**, 1705 (2003)
6 A. Efimov, A.J. Taylor, F.G. Omenetto, J.C. Knight, W.J. Wadsworth, P.St.J. Russell, Opt. Express **11**, 910 (2003)
7 A. Efimov, A.J. Taylor, F.G. Omenetto, A.V. Yulin, N.Y. Joly, F. Biancalana, D.V. Skryabin, J.C. Knight, P.St.J. Russell, Opt. Express **12**, 6498 (2004)
8 N. Akhmediev, M. Karlsson, Phys. Rev. A **51**, 2602 (1995)
9 J. Herrmann, U. Griebner, N. Zhavoronkov, A. Husakou, D. Nickel, J.C. Knight, W.J. Wadsworth, P.St.J. Russell, G. Korn, Phys. Rev. Lett. **88**, 173901 (2002)

10 W.J. Wadsworth, J.C. Knight, A. Ortigosa-Blanch, J. Arriaga, E. Silvestre, P.St.J. Russell, Electron. Lett. **36**, 53 (2000)

11 B.R. Washburn, S.E. Ralph, P.A. Lacourt, J.M. Dudley, W.T. Rhodes, R.S. Windeler, S. Coen, Electron. Lett. **37**, 1510 (2001)

12 J.H.V. Price, K. Furusawa, T.M. Monro, L. Lefort, D.J. Richardson, J. Opt. Soc. Am. B **19**, 1286 (2002)

13 F. Druon, N. Sanner, G. Lucas-Leclin, P. Georges, K.P. Hansen, A. Petersson, Appl. Opt. **42**, 6768 (2003)

14 S.O. Konorov, D.A. Akimov, A.A. Ivanov, E.E. Serebryannikov, M.V. Alfimov, K.V. Dukel'skii, A.V. Khokhlov, V.S. Shevaldin, Yu.N. Kondrat'ev, A.M. Zheltikov, Appl. Phys. B **79**, 289 (2004)

15 D.J. Kane, R. Trebino, IEEE J. Quantum Electron. **29**, 571 (1993)

16 S. Linden, H. Giessen, J. Kuhl, Phys. Stat. Sol. (b) **206**, 119 (1998)

17 N. Nishizawa, T. Goto, Opt. Express **8**, 328 (2001)

18 J.M. Dudley, X. Gu, L. Xu, M. Kimmel, E. Zeek, P. O'Shea, R. Trebino, S. Coen, R.S. Windeler, Opt. Express **10**, 1215 (2002)

19 R.H. Stolen, W.N. Leibolt, Appl. Opt. **15**, 239 (1976)

20 F.G. Omenetto, B.P. Luce, D. Yarotski, A.J. Taylor, Opt. Lett. **24**, 1392 (1999)

21 N.I. Koroteev, A.M. Zheltikov, Appl. Phys. B **67**, 53 (1998)

22 A. Efimov, A.J. Taylor, F.G. Omenetto, W.J. Wadsworth, J.C. Knight, P.St.J. Russell, CLEO/IQEC and PhAST Technical Digest on CD-ROM (The Optical Society of America, Washington, DC, 2004) IMD4